Available online at www.sciencedirect.com
SCIENCE DIRECT®
ELSEVIER
Materials Letters 57 (2003) 4394–4401
MATERIALS LETTERS
www.elsevier.com/locate/matlet

Band structure and optical properties of $LiKB_4O_7$ single crystal

P. Smok[a], H. Seinert[b], I.V. Kityk[a,*], J. Berdowski[a]

[a] *Institute of Physics WSP, Al. Armii Krajowej 13/15, Częstochowa 42200, Poland*
[b] *Institute of Electronics, University of Groningen, Gronningen, The Netherlands*

Received 27 January 2003; accepted 8 February 2003

Abstract

The band structure (BS), electronic charge density distribution and linear optical properties of the $LiKB_4O_7$ (LKB4) single crystal are calculated using a self-consistent norm-conserving pseudo-potential method within the framework of the local density approximation theory. Dispersion of the imaginary part of dielectric susceptibility as well as of density of states is found. Comparison of the theoretically calculated and the experimentally measured optical and X-ray photoelectron spectra shows a good agreement. The specific of the charge density distribution, band structure dispersion and of the optical spectra originate from two anionic groups, $(B_3O_8)^{7-}$ and $(B_5O_{10})^{5-}$ groups, forming infinite spiral chains parallel to the [100] crystallographic direction, which are interconnected by sharing oxygen atoms with $(B_5O_{10})^{5-}$ groups.

The observed behaviour of band structure is principally different from the tihium pentaborate (LBBOH) and β-BaB_2O_4 (BBO) single crystals. In the LBBOH single crystals, the anisotropy of the optical and the charge density distribution is caused by different projection of the orbitals originating from particular borate clusters on the particular crystallographic axes. In the case of the BBO, the anisotropy is caused prevailingly by a different local site symmetry of oxygen within the borate planes.

PACS: 71.15.Hx; 71.20.Ps
Keywords: Borate crystals; Band structure; Optical spectra

1. Introduction

A rapidly growing interest in borate crystals [1–7] is caused by their promising optical and nonlinear optical properties. They are just used in various quantum electronic and nonlinear optical devices. Particularly, they are widely applied as materials for laser modulators, deflectors, frequency generators and optical parametric oscillators. They possess excellent second-order nonlinear optical susceptibilities, wide spectral window of transparency (up to VUV spectral range), high laser power damage threshold, photomechanical stability, etc.

Another interesting application of the said crystals may be connected with a search of highly anisotropic optical properties in the blue spectral region [8]. This is necessary for creation of polarised optical filters, passive laser *Q* switchers and beam splitter for the blue laser. In order to produce materials possessing simultaneously good nonlinear optical properties and large anisotropy, it is necessary to clarify the origin of the connection between the electronic structure, density of states, charge density distribution and principal chemical bonds. Among borates possessing anisotropy, better known are β-BaB_2O_4 (BBO) and LiB_3O_5

* Corresponding author.
E-mail address: i.kityk@wsp.czest.pl (I.V. Kityk).

0167-577X/03/$ - see front matter © 2003 Elsevier Science B.V. All rights reserved.
doi:10.1016/S0167-577X(03)00331-8

(LBO) single crystals. In the previous works devoted to their band structures [8,9], it was shown that varying cationic subsystem and the corresponding coordination positions of oxygen within borate rings, one could change the degree of their anisotropy in the charge density distribution and the corresponding optical and electronic properties.

During the search of new highly anisotropic borates and analysing crystallochemistry of different borates, we have concerned $LiKB_4O_7$, denoted as LKB4, (space group $P2_12_12_1$) possessing two kinds of anionic group, $(B_3O_8)^{7-}$ and $(B_5O_{10})^{5-}$ [10].

Principal crystal structure of the LKB4 is shown in Fig. 1. The atoms of bor possess three or fourth coordination number with respect to the surrounding oxygen atoms. The BO_3 trigonal groups are almost planar. O–B–O bonds form bridge with angles from 105.65° to 112.4°.

The investigated crystals were grown from congruent melt in argon using Czochralski technique. The chemical purity of the materials was higher than 99.9995%. The high-quality crystals possessed sizes up to the $3 \times 3 \times 5$ mm. X-ray diffraction control has shown that the lattice parameters have the following parameters:

$a = 8.4905(11)A$; $b = 11.14149(6)A$ and $c = 12.12.6555(12)A$ with number $Z = 9$.

Comparing with other anisotropic borates (such as BBO, LBO, GdCOB,CLBO) [3,8,9,11,12] (where anisotropy originates from the different oxygen localisation within the borate ring and different interlayer stacking) in the case of the LKB4 crystals key role belongs to the $(B_3O_8)^{7-}$ groups forming infinite spiral chains parallel to the [100] direction, which are interconnected by sharing oxygen atoms with $(B_5O_{10})^{5-}$ groups. Thus, one can expect also a significant charge density anisotropy of the LKB4. The latter may be comparable with tihium pentaborate (LBBOH) [9] of the BBO or LBO. It would be important to consider an influence of this extremely complicated crystallochemistry structure on the band structure (BS) dispersion, the charge density distribution and the corresponding optical properties.

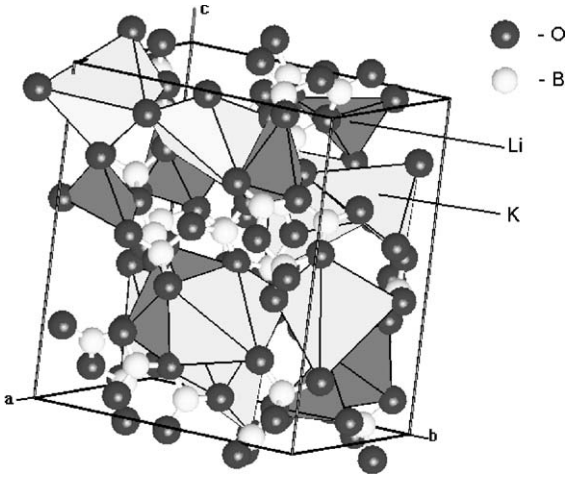

Fig. 1. General crystallochemistry of the LKB4 crystalline unit.

We compare the performed BS calculations with the data obtained from experimental optical spectra and X-ray PES density of states.

Further investigations, materials engineering modifications and applications of these materials are, however, strongly hampered by the absence of systematic studies of their BS and, particularly, the density of electronic states which is directly connected with the chemical bonds. The latter parameters are necessary for evaluation of microscopic features such as dipole moments, effective carrier masses, optical dispersion, determining the nonlinear optical parameters. Among the different calculation techniques, the norm-conserving pseudo-potential [12] scheme seems to be more useful for describing of the optical properties of borates [3,8,9].

The observed anisotropy is discussed both within the framework of BS approach as well as within the particular bonding–antibonding orbitals. To verify the calculated BS, we compared the polarised spectral dispersion of the imaginary part of the dielectric susceptibility $\varepsilon_2(E)$ calculated from the BS dispersions and the experimental one measured by ellipsometry. At the same time, the density of electronic states was measured by X-ray photoelectron spectroscopy (XPS).

2. Experimental methods

The investigated LKB4 crystals were grown from congruent melt in argon using Czochralski technique. Monitoring of the LKB4 single-crystal structure was done using a DRON 5.0 X-ray diffractometer. The

specimen's homogeneity was monitored using an optical polarisation method, which revealed that the deviation from homogeneity is less than 1.3% throughout the sample's surface.

Ellipsometric measurements were performed by a Seya-Numioka monochromator within the 3–25 eV spectral range. The specimen surfaces (2.5 × 2.5 mm) were cleaved along the mirrorlike (*bc*) planes and did not require additional treatment.

The precision of the $\varepsilon_2(E)$ evaluation was equal to about 2.3%. The samples were cleaved in vacuum of about 10^{-5} Torr. The grating monochromator allowed to make measurements of $\varepsilon_2(E)$ with spectral resolution up to 2 nm/mm. The incident UV beam angle was changed within the range 1.9–28° with respect to the normal of the cleaved surface plane. A computing program XC-130P was applied for evaluations of the $\varepsilon_2(E)$ tensor components at different incident angles. A photomultiplier operating in the single quantum calculation regime connected with a digital interface electronic boxcar integrator served for detection of the reflection light signal.

The fundamental absorption measurements were performed within the 200–350 nm range (spectral resolution about 2 A/mm). The refractive indices were measured using the spectroscopic method of Obreimow with precision better than 10^{-3} for two wavelengths: $\lambda = 337$ nm and $\lambda = 633$ nm.

The X-ray photoelectron spectroscopy (XPS) technique involves the bombardment of a sample surface with X rays and the measurement of the concomitant photo-emitted electrons. The photo-emitted electrons have discrete energies that are characteristic of the emitting atoms and their bonding states. XPS goes beyond elemental analysis to provide chemical information.

High vacuum of 10^{-10} Torr has been used. High energy resolution analyser allows to perform analysis of the photo-emitted electrons with precision up to 0.1 eV. To minimise the wave spread of the photoelectrons as they enter the analyser, we enhance precision of energy determination. The pot size has been decreased up to 31 μm. This one enables the analysis of different parts of surfaces. X-ray beams of exactly 1486.6 and 1253.6 eV impart precise energy to photoelectrons and allow accurate determination of chemical and bonding information. The use of monochromatic X rays precisely restricts the wavelength to remove satellites (associated X rays of different energies that are less intense than the primary, and preferred, X ray) from the Al Kα X-ray emission line. This ensures that the energy imparted to photoelectrons will be precise.

3. Calculation procedure

The norm-conserving pseudo-potential calculations were done within plane wave (PW) basis set. Initial structural parameters were taken from Ref. [1].

During the calculation, the following atomic wave functions were included: the occupied $2s^2$, $2p^1$B, $2s^22p^4$O, $3s^2$, $3p^4$K, $2s^2$Li valence orbitals and the excited unoccupied 3s, 3pB, 3s, 3pO, 4sK, $2p^2$Li, $2s^1$ orbitals.

The basic matrix elements of the secular equation were calculated analytically, similarly to that ones described in Ref. [13]. The calculations were done for 122 *k* points of the Brillouin zone (BZ). Electron exchange correlation screening effects were taken into account using the parametrised Perdew–Zunger [14] and Ceperley–Alder schemes [15]. The Chadi–Cohen method of special points was used for calculation of pseudo electron-charge density distribution of valence electrons. This method was applied to construct the pseudo wave-charge density function of electrons that is required for numerical evaluations of electron–electron and electron–exchange interactions during the self-consistent procedure.

Acceleration of the iteration convergence was achieved by transferring 75% of the $(m-1)$-th iteration result to the *m*th iteration. The following condition was taken as a criterion of the self-consistency:

$$|\rho_{\mathrm{out},m} - \rho_{\mathrm{inp},m}| < \varepsilon \qquad (1)$$

after the *m*th iteration step. We have assumed that $\varepsilon = 1\%$. The energy eigenvalues were stable up to 0.00089 eV and the total energy is up to 0.0005 eV. These values corresponded to the number of plane waves varying within 410–467 depending on the BZ points. The numerical evaluations of the charge density function terms were carried out using a numerical tetrahedron method with an increment equal to about 0.0059 eV. General number of iteration was equal to 16.

The calculation of the imaginary part of the dielectric susceptibility $\varepsilon_2(E)$ was performed using the expression:

$$\varepsilon_{2z,y}(E) = \frac{2\pi e^2}{mE}\int d^3\vec{k}\sum_{nl}\left\langle \psi_n(\vec{k},\vec{r})\,|\,\nabla_{z,y}\,|\,\psi_l \times (\vec{k},\vec{r})\right\rangle !^2 n_l(\vec{k})[1-n_n(\vec{k})]\delta[E_n(\vec{k}) - E_l(\vec{k}) - E] \quad (2)$$

where $\psi_n(k,r)$, $\psi_l(k,r)$ a re basic planewave wave functions for the valence and the conduction bands, respectively; $n_l(k)$ and $n_n(k)$ are occupations of the l,n band states, respectively; z,y are light polarisations with respect to the c,b-crystallographic direction. The dipole optical transition moments were calculated within the 76 k points in part of the one-eighth Brillouin zone. All the summations were carried out using the tetrahedron methods.

4. Results and discussion

Our calculations have shown that for achievement of sufficient total energy and eigenstate convergence, it was necessary to have a cutoff energy level equal to about 35 Ry. During the calculations, we varied also the starting structural parameters a, b and c (up to $\pm 3.2\%$) comparing with initial experimentally measured structure [10] to find the total energy minimum (optimisation of structure). Our calculations showed that the optimised crystalline structure corresponded to the lattice parameters: $a = 8.4904$ A, $b = 11.1411$ A and $c = 12.6189$ A. Thus, the error obtained for the theoretical volume compared with the experimental one is typical that of the LDA methods within the DFT approach. These parameters were used during the structural factor's evaluations. We have found that the bulk modulus is equal to about 12.89 Pa^{-1} which is in a good agreement with the experimental data (12.77 Pa^{-1}) [16]. A general view of the LKB4 BS calculated within the above-described method is presented in Fig. 2. One can see that the BS dispersion E (k) is rather flat (except the X–Γ–R BZ directions), and band level crossing is relatively low. Moreover, the observed k dispersion is similar both for the valence band states as well as for the

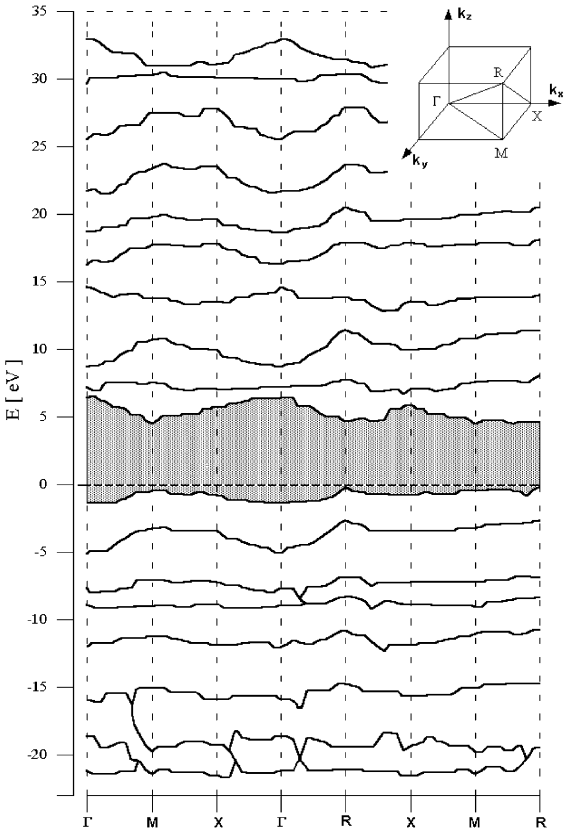

Fig. 2. Main symmetry points in the first BZ of LKB4 single crystals and band structure calculated within the BHS model.

unoccupied conduction band states. Another important factor is an indirect type of the band energy gap, E_g (the top of the VB is situated at the R BZ point and the bottom of the conduction band at the M BZ point), which is equal about 4.87 eV. This is in accordance with the experimental measurements of the band absorption edge, where steplike phonon repetitions were observed (which indicate on indirect absorption edge). The calculated E_g is only about 0.62 eV less than the experimentally measured 5.49 eV. The underestimation of the energy gap is typical for the DFT calculations.

One of the specifics of the observed band dispersions is in the appearance of the discontinuities near the symmetry point. It is similar to the BS dispersion done in the other borate crystals [3,8,9,11,12] and may reflect relatively strong interaction of two anionic groups, $(B_3O_8)^{7-}$ and $((B_5O_{10})^{5-}$.

We have performed simulations of the imaginary part of the dielectric susceptibility $\varepsilon_2(E)$ for the non-polarised case and compared the calculations with the obtained experimental ellipsometric data.

The corresponding results are presented in Fig. 3. From Fig. 3, one can clearly see that experimental values of $\varepsilon_2(E)$ are shifted towards higher spectral energies as compared with $\varepsilon_2(E)$ up to the 0.8 eV. This is in accordance with the shift of the energy gap value as mentioned above. To understand the origin of the observed $\varepsilon_2(E)$ behaviour, we have calculated transition dipole moments in determining $\varepsilon_2(E)$ (see Eq. (2)) vs. the $\boldsymbol{k}$ vector of the BZ.

The calculations were done for the valence and the conduction bands which effectively contribute to the observed spectra and to the interband distances below 16 eV.

Comparison of Fig. 4a, b and c shows a significant anisotropy of the transition dipole dependencies for different light polarisations. Only the ΓM BZ line shows a little similarity. For all the others directions, dipole matrix elements for the p_y are higher than for the p_z. This leads to the substantial anisotropy of partial contributions originating from different sub-bands and may explain occurrence of the extremely large energy dispersion nearby the symmetry points. Particularly, it is clear in the $\Gamma-R-X$ direction of the BZ.

Our calculations have shown that the main contribution to $\varepsilon_2(E)$ gives $R-\Gamma-X$ direction of the BZ.

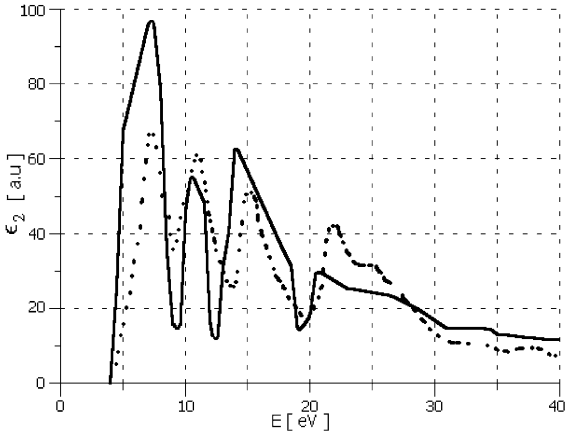

Fig. 3. Theoretically simulated spectral dependencies of the imaginary part of dielectric susceptibility. Experimental dependence is indicated by dotted line.

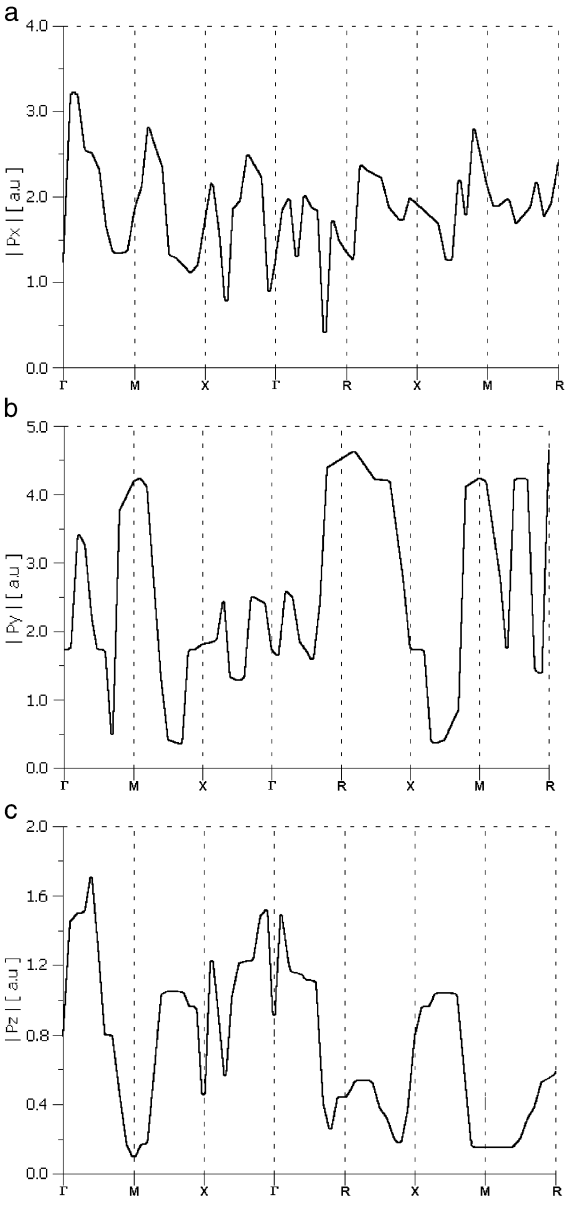

Fig. 4. Distribution of the transition dipole moments through the BZ: (a) p_x; (b) p_y; (c) p_z corresponding to interband energy distances below 16 eV.

Depending on the relative contribution of the particular structural borate fragments to the BZ directions, we have revealed that the coordination's disturbance of oxygen within the borate rings is not so crucial for the splitting of the BS levels as in the case of BBO and LBO [8–11]. This is in an agreement with the BZ

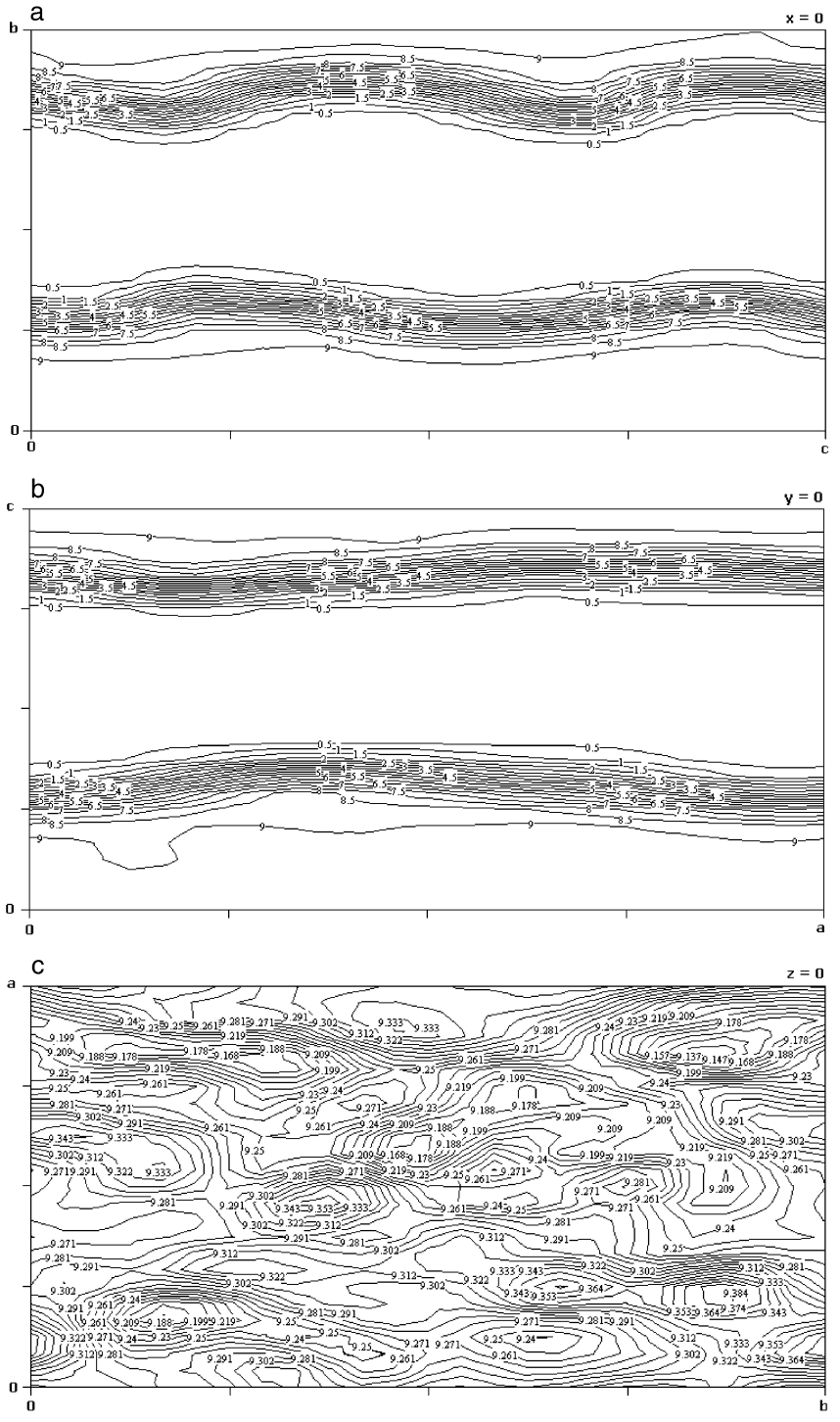

Fig. 5. Charge–density distribution in the LKB4 on the: (a) ⟨011⟩ at $a=0$; (b) ⟨101⟩ at $b=0$; (c) ⟨110⟩ at $c=0$. The contour lines are from 0.02 to 0.30 by 0.005 in units/a.u.$^{-3}$.

splitting of the upper valence band in the $M–X–\Gamma–R$ and the $X–M$ BZ directions.

The main origin of the observed $\varepsilon_2(E)$ behaviour is caused by a different projection of the bonding $2p_{x,y}B–2p_{x,y}O$ states (forming prevailingly the upper v.b.) on particular directions of the BZ due to specific stereochemistry of the LKB4 (Fig. 1).

The second groups of the levels originate from the deeper 3pK atoms (lower valence band) [3,9]. The good agreement of the calculated and the measured $\varepsilon_2(E)$ spectra may show on a good level of the adopted theoretical model.

For evaluations of the atomiclike origin of particular bands, we have used the band projection procedure from the plane wave basis set to the localised orbitals particularly described in Ref. [13].

In Fig. 5, the pseudo charge-density distributions for different crystalline sequences are shown. One can see substantial anisotropy of the charge density distribution for the crystalline ⟨011⟩ (Fig. 5a), ⟨101⟩ (Fig. 5b) and ⟨110⟩ cuts (Fig. 5c). For convenience, the cuts are done at $x=0$ and $y=0$ and $z=0$ planes and, even without a charge density gradient calculations, one can see a large charge-density anisotropy.

Finally, Fig. 6 presents the calculated DOS spectra and compares it with the experimentally measured ones. One can see a confirmation of the ellipsometric data presented in Fig. 3. The latter may be an independent confirmation of sufficient role played by the said borate clusters.

Comparing the calculated BS of the LKB4 with the ones for other borates, one can see substantial differences in the band's dispersion behaviour [3,8,9]. The LKB4 crystals have a larger BS dispersion, along the $\Gamma–M–X$ directions of the BZ. The performed calculations show that the latter is caused by a substantial hybridisation of the covalence bonding–antibonding 2pO–2pB chemical orbitals originating from the said two borate anionic groups, giving different contributions in different BZ directions and specific influence of the Li and K cations.

Comparing with other borate crystals [3,6,8,9], it is necessary to emphasise that difference in the BS k dispersion are the main sources of the observed optical and DOS features. Appropriately changing positions of light (Li) and relatively heavy (K) cations, one can operate on the corresponding mobility of valence electrons. For the optical properties, such changes of effective masses cause corresponding changes in the transition dipole moments. However, recently, we have done the calculations for the isostructural Ba pentaborate crystals [9]; the discontinuities in the bands are similar to the observed in the LKB4 crystals.

The appearance of the anisotropy in LKB4 is enhanced additionally by weak $2p_yO–2p_yO$ antibonding bonds (similar to weak van der Waals bonds)

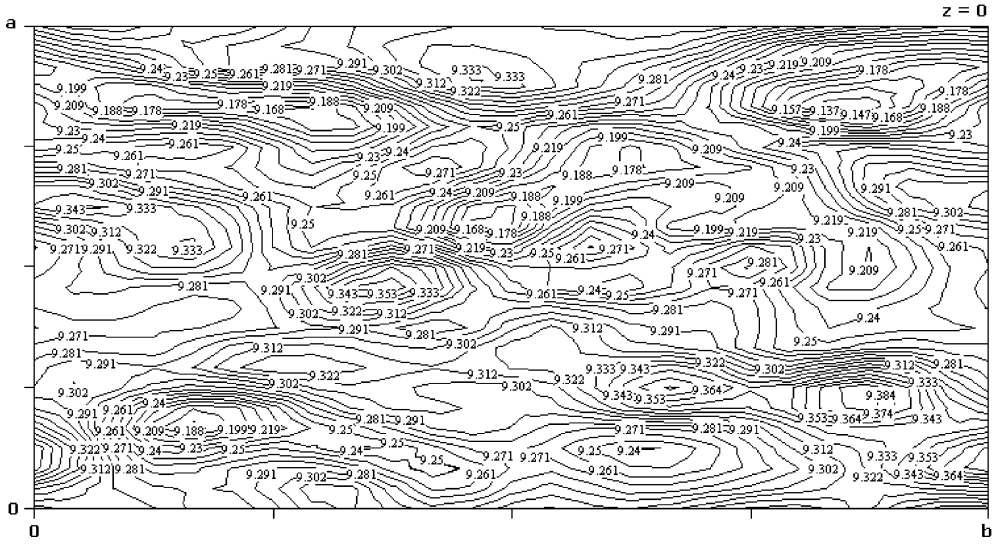

Fig. 6. Density of states distribution of the LKB4 measured from X-ray PES spectra. Presented by dotted lines are experimental dependencies.

originating from oxygens belonging to the neighbouring borate rings (see Fig. 1).

The space electron charge density gradient shows a huge level of anisotropy (see Fig. 5). For example, for the intraborate band for ⟨001⟩ BZ direction, this derivative is equal to 20 e/Ω A and for the direction with prevailingly interborate chemical bonds equal to 103 e/Ω A. This fact indicates that in order to modify the LKB4 in desirable direction, it is necessary to modify the packing of the particular borate rings in a such a way to achieve a large degree of anisotropy in orbital distributions. Only a manipulation by oxygen within the borate rings or due to interlayer van der Waals forces is not sufficient enough for substantial enhancement of the anisotropy. To obtain a space separation of particular borate planes, it is necessary to have additional molecular groups favouring a separation of the said borates. For the LKB4 crystals, such anisotropy may be achieved by appropriate forming of infinite spiral chains parallel to ⟨100⟩ direction, which are interconnected by sharing oxygen atoms with $(B_5O_{10})^{5-}$ groups.

5. Conclusion

Using self-consistent nonlocal norm-conserving pseudo-potential calculations, we have performed calculation of imaginary part of dielectric susceptibility of LKB4 within the spectral range 3–30 eV. Besides particular contributions of the transitions, dipole moments were evaluated. Comparison with the experimental ellipsometric and the X-ray data shows a sufficient agreement. The band dispersion is similar to the pentaborate crystals; however, the LKB4 crystal shows extremely high k dispersion in the relatively deeper bands in the Γ–M and the X–Γ–R BZ directions.

This is confirmed by substantial anisotropy of contribution of different subbands. A good agreement of the theoretically calculated $\varepsilon_2(E)$ and the DOS spectra with the experiment may be an additional proof of the obtained dependencies.

References

[1] L.K. Cheng, W. Bosenberg, C.L. Tang, J. Cryst. Growth 89 (1988) 553.
[2] C.T. Chen, Y. Wu, A. Jiang, B. Wu, G. You, R. Li, S. Lin, J. Opt. Soc. Am. B 6 (1989) 616;
C.T. Chen, B.C. Wu, A.D. Jiang, Sci. Sin., Ser. B 28 (1985) 234.
[3] T. Łukasiewicz, A. Majchrowski, I.V. Kityk, J. Kroog, Mater. Lett. 57 (2002) 130;
I.V. Kityk, P. Smok, J. Berdowski, T. Łukasiewicz, A. Majchrowski, Phys. Lett. A 280 (2001) 70.
[4] Y. Mori, I. Kuroda, T. Sasaki, S. Nakai, Jpn. J. Appl. Phys. 34 (1995) L296.
[5] G. Zhang, Y. Wu, P. Fu, G. Wang, H. Liu, G. Fan, C. Chen, J. Phys. Chem. Solids 63 (2002) 145.
[6] G. Aka, A. Kahn-Haradi, D. Vivien, J.-M. Benitez, F. Salin, J. Godard, Eur. J. Solid State Inorg. Chem. 33 (1996) 727;
I.N. Ogorodnikiov, V.A. Pustovarov, A.V. Kruzhalov, L.I. Isaenko, M. Kirm, G. Zimmerer, Phys. Solid State 42 (2000) 1846.
[7] P. Becker, Adv. Mater. 10 (1998) 979.
[8] P. Smok, I.V. Kityk, J. Berdowski, Physica B 328 (2003) 163.
[9] P. Smok, I.V. Kityk, K.J. Plucinski, J. Berdowski, Phys. Rev., B 65 (2002) 205103.
[10] Y. Ono, M. Nakaya, T. Sugawara, N. Watanabe, H. Siraishi, R. Komatsu, T. Kajtani, J. Cryst. Growth 229 (2001) 472.
[11] R.H. French, J.W. Ling, F.S. Ohuchi, C.T. Chen, Phys. Rev. 44B (1991) 8496;
Y.-N. Xu, W.Y. Ching, R.H. French, Phys. Rev., B 48 (1993) 17695.
[12] G.B. Bachelet, D.R. Hamann, M. Schluter, Phys. Rev., B 26 (1982) 4199.
[13] I.V. Kityk, B.V. Andriewskii, J. Kasperczyk, Phys. Lett. 216A (1996) 161.
[14] J.B. Perdew, A. Zunger, Phys. Rev., B 23 (1981) 5048.
[15] D.M. Ceperley, B.J. Adler, Phys. Rev. Lett. 45 (1980) 161.
[16] X. Pimenov, L. Isaenko, Structural Data, Ref., Ed. Technika, St-Petersburg, 1999, p. 156.